VECTORCARDIOGRAPHY BASED ANALYSIS OF ATRIAL FIBRILLATION

A. van Oosterom

Department Cardiomet, Faculty of Biology and Medicine, University of Lausanne, Lausanne Switzerland
e-mail: Adriaan.vanoosterom@epfl.ch

This paper discusses the feasibility and effectiveness of using vectors of the current dipoles representing local electric activity inside the atrial myocardium during atrial fibrillation. The application relates to the search for improving the performance of electric signals observed on the body surface in the diagnoses of this life-threatening arrhythmia. The topics addressed include some historical and basic conceptual notes on the use of the vector, as well as some recent developments in which the vector concept is used in combination with spectral analysis. The invited paper is of a didactic nature.

Published in: Electrocardiology 2009; pp: 39-55; Proc 36th Int Congress on Electrocardiology Wroclaw, Poland, Edts: M. Sobieszczańska, J. Jagielski and P.W. Macfarlane; JAKS Publishing Company 2010.

Typos corrected: 2010_04_27

INTRODUCTION

Atrial fibrillation (AF) is the most frequently observed arrhythmia in the human heart. While it clearly causes discomfort in patients, it has long been believed to be relatively harmless and, unlike ventricular fibrillation, it is not immediately life threatening. However, of late it has become clear that AF often leads to severe complications such as heart failure and stroke due to blood clot formation in the atrial appendices [1]. The prevalence of AF increases with age. With the present increase in lifetime expectancy in the western population, interest in the analysis of the causes of AF has become one of the focal points of current research [2].

AF can have different origins, ranging from viral infections to thyrotoxicosis. The clinical classification of AF is mainly restricted to distinguishing between paroxysmal, persistent and permanent types [3]. Invasive, electrophysiological studies have identified different mechanisms involved in the initiation of AF and how it may be sustained. In one frequently observed variant, AF is sustained by spontaneous activity in the region around the pulmonary veins [4]. Other types include spontaneous focal activity that may be located in one or more various locations in the left and/or the right atrium. Mechanisms that have been proposed as causing sustained AF include inhomogeneities in the electric coupling of atrial myocytes or their basic ion-kinetics.

Current therapies for treating AF include: pharmaceutical therapy, electric cardioversion (electric shock), the introduction of ablation lines on the atrial endocardium by means of catheters or, in extreme cases, surgical intervention.

The research discussed here is motivated by the quest for an optimal classification of the different types of AF on the basis of atrial signals recorded on the body surface. This improved classification would facilitate the selection of an optimal therapy.

On Modeling

When interpreting the electric signals arising from the heart's activity invariably two separate types of models are involved. One deals with the specification of the (active, primary) electric current sources generated at or near the membranes of cardiac cells: the source model. The other is the volume conductor model, which describes the effects of the (passive) electric properties of the tissues surrounding the primary sources on the potential differences between the two poles of any lead system. While interpreting observed ECG wave forms, most cardiologists (and electro-physiologists) are usually not aware of these separate factors and they perform a mental signal analysis on the observed data, based on past experience. Some even claim not to believe in the usefulness of modeling. However, the complexity of the problem involved, in particular that related to the interpretation of AF signals, is so enormous that when trying to stretch the diagnostic performance of ECG-based techniques both factors (model elements) need to be included.

The model-based approach to the interpretation of the ECG consists in the solving of the so-called Inverse Problem of electrocardiography [5]. A pre-requisite for its solution, demanded by the nature of the physics of the flow of electric currents inside conductive media (tissues), is the formulation of an appropriate, dedicated source-volume conductor model. Based on the latter, the (forward) transfer between the primary current sources and the resulting potentials can be computed, a procedure known as solving the (associated) Forward Problem [6-8]. By using numerical techniques, the solution of the forward problem as such is straightforward. The solution to the problem of clinical interest, the inverse problem, which involves taking the inverse of the computed forward transfer, is generally more complicated.

The Symposium on Vectorcardiography is dead; long live the dipole source vector!

This paper was presented during the 36th International Congress on Electrocardiology, which also was announced as the 50th International Symposium on Vectorcardiography. Prior to this meeting, the Council of the International Society on Electrocardiology decided that for future annual meetings the subheading: International Symposium on Vectorcardiography would no longer be carried. The motivation for this does not reflect a lack of "confidence" in the usefulness of the vector in diagnostic procedures, but rather that it was felt that it would do more justice to the other, more recent sub-specialities of electrocardiology, such as body surface potential mapping (BSPM) and advanced methods of cardiac imaging. Beside the previously proven quality of the vectorcardiogram (VCG), in particular in the hands its experts, and its usefulness in the basic concepts of ECG interpretation, the results shown in this paper suggest that the vector concept may be decidedly useful in the interpretation of AF signals.

Outline

The outline of this paper is as follows. First, a brief characterization of the vector concept is given, against the background of some historical notes. Second, the complexity of the primary atrial sources is discussed, in particular those during atrial fibrillation. This is followed by an illustration of when and how the vector representing a current dipole might be useful. Finally, some recent results from studies in which these concepts have been tested in an application to simulated AF signals are discussed.

VECTORCARDIOGRAPHY

The current dipole

The electric current dipole is probably the best-known model of the cardiac electrical generator. It forms the basis of vectorcardiography (VCG). In Einthoven's papers, e.g. [9] , we see it appearing as

an arrow drawn on a plane, representing the "electromotive force " of the heart (right panel of Figure 1). The location of the implied current dipole source is at the center of the arrow. Just below it, marked by a + sign, an electric current is injected into the surrounding medium; the location is referred to as the source of the dipole. Just above it, marked by a – sign, exactly the same current is withdrawn from the medium; the location is referred to as the sink of the dipole. The nature of the current dipole can be likened to that of a circulation pump inside an aquarium: the flow of water does not alter the

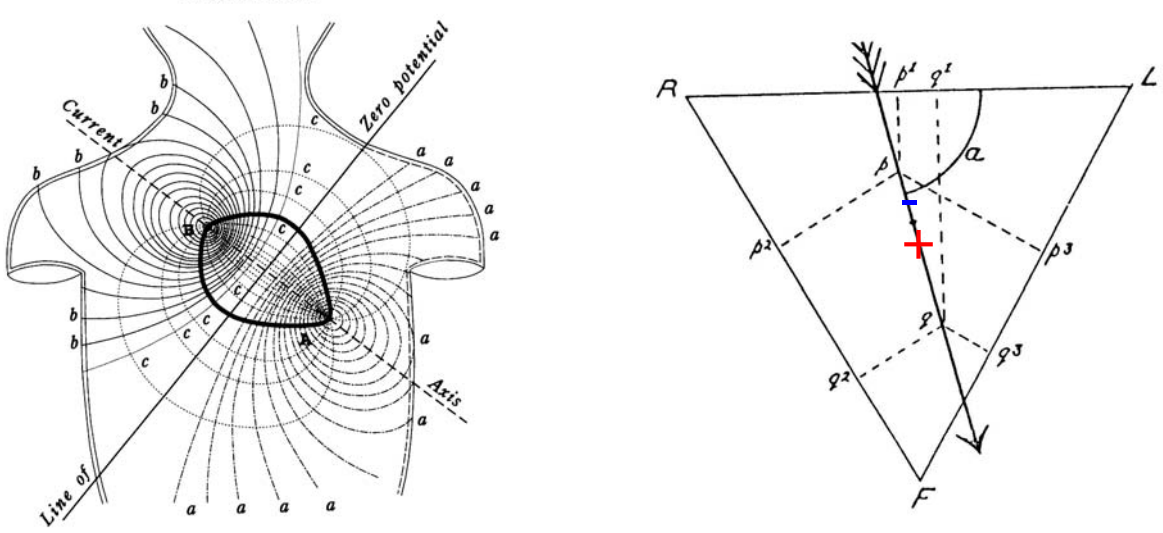

Figure 1. Left panel: Potential field lines (solid) and current density lines (dashed) drawn on the frontal plane of the thorax, generated by a current dipole, oriented along the Current Axis toward the right arm, placed at the intersection between the zero potential line and the Current Axis (Waller 1887). **Right panel:** current dipole appearing in the work of Einthoven (18913), drawn at the center of an equilateral triangle, the vertices of which represent: right arm R, left arm L, and (left) leg F.

(water) volume inside the aquarium. In the same manner, the current dipole does not affect the total electric charge in the thorax.

The dipole concept is also evident in an even earlier paper, the one by Waller, published in 1887 [10] (left panel of Figure 1). The potential field lines relate to a volume conductor model of uniform electric conductivity σ (unit: [S/m]) and having an infinite extent. In spite of the clear lack of realism of the depicted field (current lines should not cross the thorax boundary) the figure captures the most prominent, global features of the potential field observed on the thorax. The zero reference for the potential is defined at infinity. By placing the origin at the dipole location, the value of the potential ϕ at any field point in space is inversely proportional to the square of the distance R, which is the length of the vector $\vec{R}$ (with components [x, y, z]) pointing from source location to observation point. Moreover, the potential is linearly proportional to the cosine of the angle α between the current axis and the line drawn from source location to field point [x,y,z]:

$$\phi(x,y,z) = \frac{D}{4\pi\sigma}\frac{\cos\alpha}{R^2} = \frac{1}{4\pi\sigma}\frac{D_x x + D_y y + D_z z}{R^3} \qquad (1)$$

with D (unit [A m]) denoting the strength of the current dipole , $\vec{D}$, with vector components in 3D space: [D_x , D_y , D_z]. This expression holds true if R is much greater than the distance between the current source and sink. In this paper, the convention is used of defining the x, y, z directions as pointing anteriorly, to the left and to the head, respectively.

The same expression applies to the configuration used by Einthoven (right panel of Figure 1), while assuming the dipole placed in infinite space and defining the potential (reference) at infinity as zero, as well as when using the more realistic assumption of a homogeneously conducting sphere bounded by air, centered around the dipole location, and *defining* the mean potential over the surface of the sphere as zero [11, 12]. If the field points R, L and F lie on the sphere, the potentials values at R, L, and F in the bounded situation are threefold those of the unbounded sphere.

The above treatment is included here as representing the simplest example of handling source-volume configurations. The solution (1) to the "Forward Problem" involved is the one found by using classic, analytical methods [13].

From the expression on the right of (1) it can be seen that for any known dipole-field point configuration $\vec{R}$, the potential at the field point is a linear combination of the components of the dipole vector $\vec{D}$, a weighted sum, with weights:

$$[w_x, w_y, w_z] = [\frac{x}{4\pi\sigma R^3}, \frac{y}{4\pi\sigma R^3}, \frac{z}{4\pi\sigma R^3}] \quad . \tag{2}$$

Accordingly we may reformulate (1) as

$$\phi(x, y, z) = w_x D_x + w_y D_y + w_z D_z \tag{3}$$

The three weights, [w_x, w_y, w_z], are independent of the dipole *strength*; they can be viewed as the components of a vector $\vec{w}$ in 3-D space. The linear combination expressed by (3) is known as the scalar product of vectors $\vec{w}$ and $\vec{D}$. The vectors $\vec{w}$ are referred to as lead-vectors: for any fixed dipole location they are functions of the positions of the electrodes involved in recording any ECG lead considered [14] . Since $\vec{R}$ depends also on the dipole location, the lead-vectors are dipole-location specific.

For the simple source-volume conductor, the corresponding "Inverse Problem" entails the computation of the three source dipole components of the basis of observed field potentials. Since (3) constitutes a single linear equation in the three unknowns, [D_x , D_y ,D_z], their solution demands at least three such equations, each related to the potential observed at a different field point. For the configuration implied on the right panel of Figure 1, such a set of equations, based on the potentials at field points [R, L,F], and the three lead-specific lead-vectors are

$$\begin{aligned} \phi_R &= w_{R;x} D_x + w_{R;y} D_y + w_{R;z} D_z \\ \phi_L &= w_{L;x} D_x + w_{L;y} D_y + w_{L;z} D_z \\ \phi_F &= w_{F;x} D_x + w_{F;y} D_y + w_{F;z} D_z \end{aligned} \tag{4}$$

For the infinite medium, with the potential at infinity defined as zero, this set of equations suffices, but only since there is an implied fourth equation: the zero potential reference potential at infinity implied in equation (1). For the more realistic, bounded medium, with electrodes sensing the potential, at least four electrodes need to be used, since –in the forward sense- the mean potential over the bounded medium (body surface) is not related to the internal current source distribution. Only in the situation where all electrodes are coplanar and the dipole has its components in the same plane only (again, as in Figure 1) can the solution be found on the basis of using just three electrodes, with one, or an arbitrary linear combination of the potentials at all electrodes serving as the reference.

For a medium bounded by the complex shape of the thorax, lead-vectors can be computed by means of numerical methods [7]. For L electrode positions, the solution to the forward problem can be expressed as a matrix multiplication specified in (5) b, in which $V_\ell = \phi_\ell - \phi_{\text{ref}}$, the difference of the potential at the sensing electrode ℓ with respect to any terminal acting as the reference.

$$\begin{bmatrix} V_1 \\ . \\ V_\ell \\ . \\ V_L \end{bmatrix} = \begin{bmatrix} w_{1,x} & w_{1,y} & w_{1,z} \\ . & . & . \\ w_{\ell,x} & w_{\ell,y} & w_{\ell,z} \\ . & . & . \\ w_{L,x} & w_{L,y} & w_{L,z} \end{bmatrix} \begin{bmatrix} D_x \\ D_y \\ D_z \end{bmatrix} \quad (5)$$

An even more compact notation reads

$$\mathbf{V} = \mathbf{W}\ \mathbf{D} \quad (6)$$

in which the rows of the matrix **W** represent the lead-specific transfer coefficients found by solving the Forward Problem: the lead-vectors. This notation stems from the field of linear algebra, in which any set of L scalar values is referred to as a vector (in L-dimensional space). The corresponding solution of the inverse problem can be formulated as

$$\mathbf{D} = \mathbf{M}\ \mathbf{V} \quad (7)$$

in which $\mathbf{M} = \mathbf{W}^{-1}$ denotes the (pseudo) inverse of the forward transfer matrix.

If the physical reality of the problem studied is indeed that of a single dipole placed inside a bounded medium whose volume conduction aspects (geometry, conductivity) are known exactly, present day numerical methods will produce a highly accurate inverse solution [15].

Vectorcardiography

In vectorcardiography the source-volume conductor model involved is that of a single current dipole at a fixed location in space, whose vector of time-varying elements, $[D_x(t), D_y(t), D_z(t)]$, are taken as a global representation of the entire spatio-temporal complexity of the heart. These elements are estimated from a limited set of leads. The estimates are generally referred to as the orthogonal leads $X(t)$, $Y(t)$ and $Z(t)$, which can be viewed by plotting them as a function of time, just like the commonly used display of the standard 12-lead signals. Different visualizations of the spatio-temporal nature of these results have been employed, such as the full trajectory of the locus of the (arrow-head of the) vector as a function of time, the projection of the latter trajectory on a spherical surface (polar cardiography [16]), or its projection on the frontal, horizontal or transverse planes, the so-called vector loops.

It is this intrinsic spatio-temporal nature of the VCG that is one of the specific advantages of the VCG over the 12-lead ECG. Other such advantages are that the estimated vector is independent of the particular potential reference involved, independent of heart position and independent of scaling [17]. These advantages emerge clearly only if the quality of estimation of the dipole strength (the inverse problem, equation (7)) is sufficient.

The optimum dipole estimate, consistent with the implied modeling assumptions: a single source dipole and a uniformly conducting medium with tailored thorax geometry, would demand a complete specification of the potential field over the thorax surface [18].

In the practical application of vectorcardiography, most of the above conditions are not satisfied, since:

1. the involved electric source is that of a volume source density throughout the myocardium rather than a single dipole,
2. the thorax geometry implied in the transfer is not tailored, but standard,

3. the electric conductivity of the thorax is not homogeneous; e.g. lungs and blood-filled compartments have electric conductivity values that differ considerably from those of surrounding tissues,
4. the potential field on the thorax is generally sampled spatially at a limited number of electrode sites.

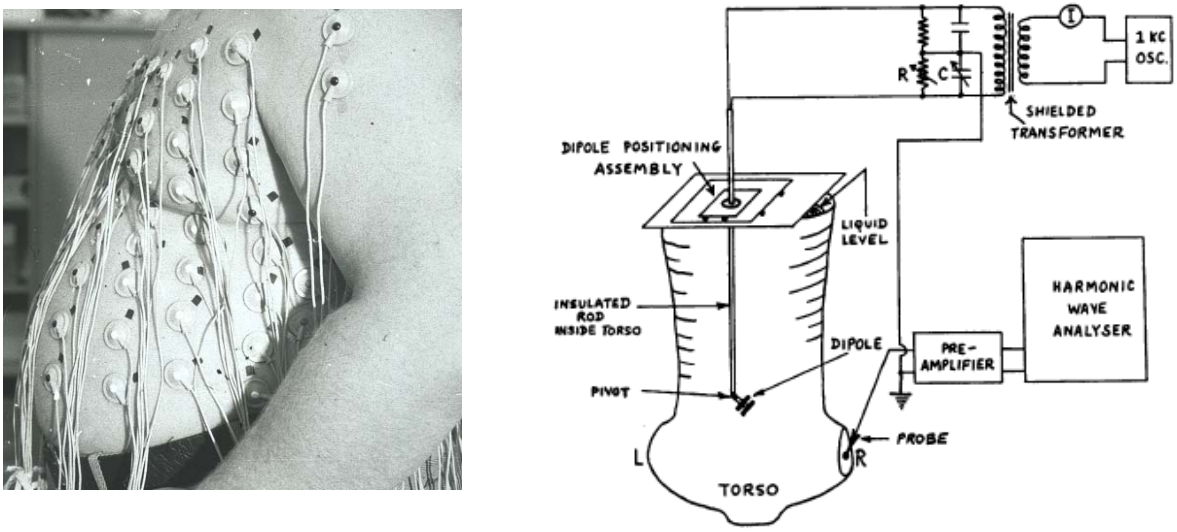

Figure 2. Left panel: The THIRD dimension of volume conduction inside the thorax. **Right panel:** Frank solving the Forward Problem; a schematic diagram of the tank model used by Frank and Kay while devising the "Frank-lead system" [19]

In the past, a major research effort has been devoted to devising lead systems (electrode montages) and associated lead-field matrices **W** such that the dipole **D** estimated on the basis of (7) might be effective in diagnostic applications (for an overview: see [20]).

In the follow-up to Einthoven's analysis, essentially restricted to the frontal plane (2-D), it was recognized that the third dimension of the thorax should also be included (left panel Figure. 2). This was stressed by, amongst others, Burger and van Milaan [21].

The most commonly used electrode montage is the one devised by Frank [22]. It employs seven electrodes, placed at heuristically selected positions on the thorax. The lead-vectors were determined by placing a current dipole-like source configuration inside a tank-shaped thorax model (right panel, Figure 2), placed successively at 60 locations in the region of the heart, and at each location oriented successively in the x, y, and z direction [19]. For each of these 180 source configurations the differences between potentials with respect to the common reference electrode were measured at 200 electrodes evenly distributed over the surface of the tank. Subsequently, by analyzing the resulting lead-vectors, a matrix **M** was devised, of size 3×7. The implementation of the matrix was realized through a network of 13 resistors, weighting the potentials at the electrode sites, directly producing the estimates of the strength of the three dipole elements at three specific terminal pairs. The matrix representation, **M,** of the action of the resistor network is (Equation 2 in [22])

$$\mathbf{M}_{\mathrm{F}} = \begin{bmatrix} 0.61 & 0.17 & 0 & -0.781 & 0 & 0 & 0 \\ 0 & 0 & 0 & 0. & 0.345 & -1 & 0.655 \\ 0.133 & -0.231 & -0.374 & -0.264 & 0.763 & 0 & 0 \end{bmatrix} \tag{8}$$

The seven elements of each row of this matrix are used to form a linear combination of the potentials observed at seven electrodes [A C E I M H F], related to, for rows 1-3, the dipole directions pointing to 1) the left arm, 2) the feet and 3) the back, respectively. Note that the sum of the elements of each row is zero. This property ensures that the dipole estimates are independent of any electrode serving as the potential reference. The positions of electrodes [A C E I] in the horizontal plane, as

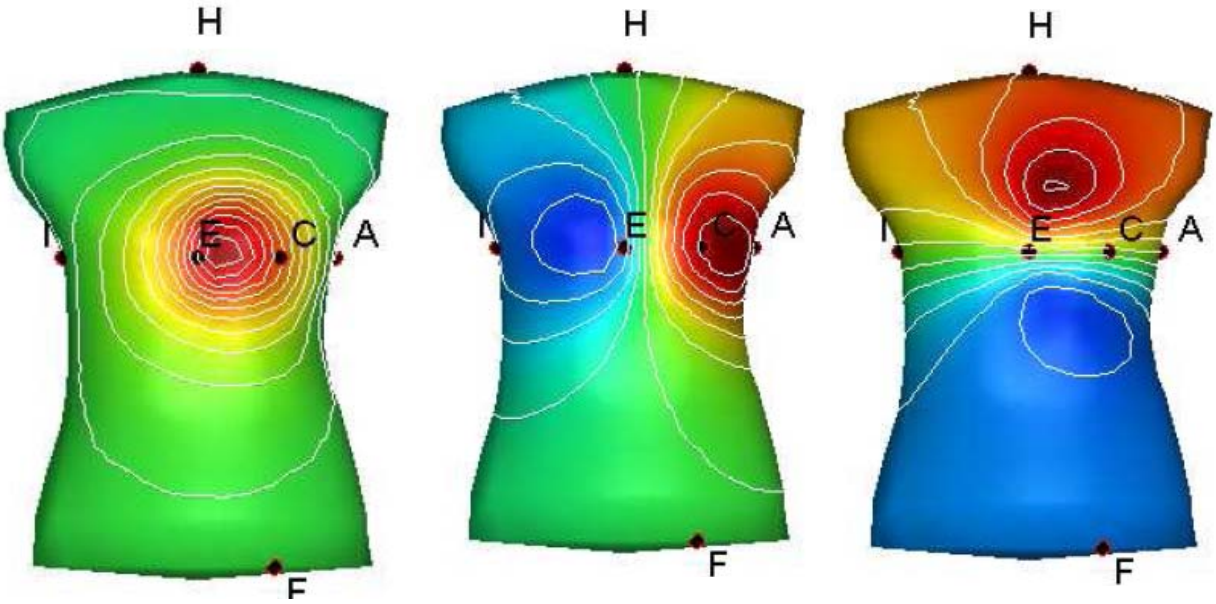

Figure 3. Potential fields on the anterior part of a numerical replica of Frank's tank model, generated by unit current dipoles at the centre of ventricular mass, oriented in the **left panel:** to the front, in the **middle panel**: to the right**,** and in the **right panel:** to the head. Positions of six of the Frank electrodes as indicated; the remaining one, electrode M, is located on the back, directly opposite electrode E. The potential steps between subsequent equipotential lines (0.2 in arbitrary units (a.u)) are equal in all three images. Local potential maxim, those near electrodes E, C and halfway in between electrodes E and H, are 21.7, 13.6 and 14.2 (in a.u.), respectively.

well those of the head electrode (H) and left leg electrode [F], are shown in Figure 3. The seventh electrode is on the back, on the same level as that of electrodes [A C E I].

Frank's matrix has been generally adopted as the gold standard of vectorcardiography. The fixed dipole location for which $\mathbf{M}_F$ was optimized, was that of the center of mass of the ventricles observed in the individual subject studied. The errors resulting from a non-matching dipole location at any of the 60 sites measured and the one involved in $\mathbf{M}_F$ were documented by Frank.

These days, the evaluation of the effect of modeling errors can be carried out easily by means of numerical methods. A demonstration of the effectiveness of this method is as follows. Based on the geometry of the thorax specified in Frank's paper, its numerical, triangulated variant was created. The three potential fields on the (bounded) thorax (tank) surface, generated by unit-strength current dipoles, oriented at each of the orthogonal directions [*x, y, z*] , located at the same reference position (center of ventricular mass) as used by Frank, were computed using the boundary element method (BEM) [7, 15]. The resulting potential fields are shown in Figure 3. Note that the spatial sampling of the potential fields is not intuitively optimal.

For each of the three dipole orientations, the potentials at the seven Frank electrodes were stored as columns in a lead-field matrix **W** (size: 7×3); its three columns were shifted to zero-mean in order to

ensure independence of the potential reference [23]. The corresponding numerically computed inverse matrix $\mathbf{M}_n$ was taken to be the pseudo-inverse of (the shifted) matrix $\mathbf{W}$. The result, matrix $\mathbf{M}_n$, is documented by equation (9), in a version to which an overall scaling was applied such that the inversely computed dipole strengths were as close as possible, in the least squares sense, to the same

$$\mathbf{M}_n = \begin{bmatrix} 0.323 & 0.407 & -0.300 & -0.252 & -0.081 & -0.077 & -0.020 \\ -0.043 & -0.026 & -0.067 & -0.025 & -0.002 & -0.715 & 0878 \\ 0.125 & -0.235 & -0.383 & 0.089 & 0.217 & 0.085 & 0.102 \end{bmatrix} \quad (9)$$

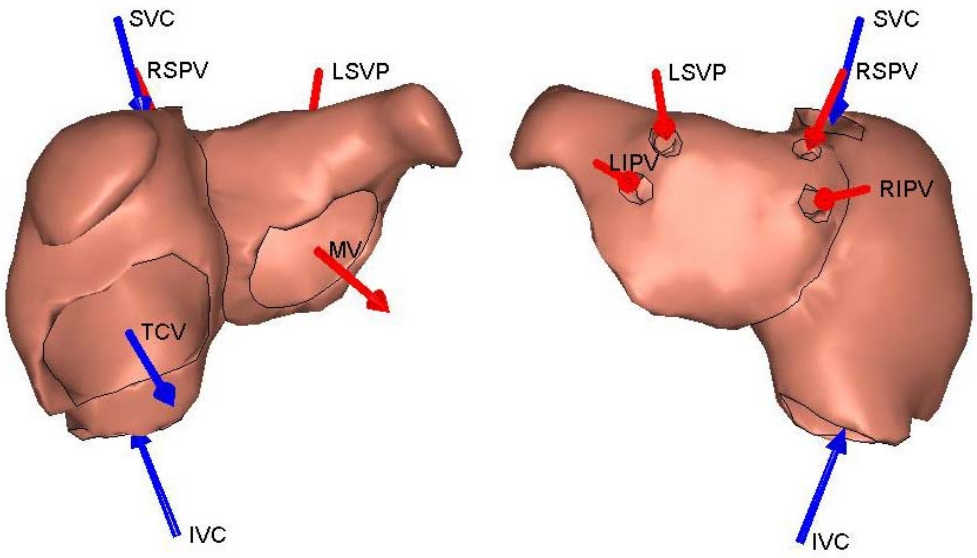

Figure 4. Geometry used in this paper of the atria as derived from magnetic resonance imaging, with the heart in its natural position [24]. **Left:** frontal view; **Right**: posterior view. The arrows shown mark the locations where the blood enters and leaves the atrial cavities. The labels denote: MV: mitral valve; TCV: tricuspid valve; IVC: inferior vena cava, SVC: superior vena cava; LSPV: left superior pulmonary vein; LIPV: left inferior pulmonary vein; RSPV: right superior pulmonary vein; RIPV: right inferior pulmonary vein; The opening marked as TCV represents both the non-propagating region of the right atrium: the tricuspid valve as well as the right ventricular outflow track.

type of results based on $\mathbf{M}_F$. Following the production of the numerical specification of thorax geometry, and the computation of the matrix expressing the effects of the boundary (demanding just a few seconds), the computation of $\mathbf{M}_n$ takes less than a second when carried out on any lap- or desktop computer.

A quality measure Q, defined as the ratio of the root mean square differences between the actual dipole elements (the ones used when designing the matrices $\mathbf{M}$) and the estimated ones, relative to the root mean square values of the latter. In the application to the potential fields simulated for the three orientations of the source dipole, the value of Q of the inverse solution based on $\mathbf{M}_n$ was 1 (perfect) , when using $\mathbf{M}_F$ it was 0.83. This lower value is partly due to the sparseness of matrix $\mathbf{M}_F$, a property that was a highly advantageous matrix property when (in 1956) the weighting could only be implemented by means of a resistor network.

ATRIAL ELECTRIC SOURCES

During the last decade, the members of the Lausanne Heart Group (www.lausanneheart.ch) have been engaged in the development of an activation model capable of simulating the activation patterns during normal activation, atrial flutter (AFL) and AF. The research was initiated by Prof. Lukas Kappenberger, motivated by his firm belief that the analysis of the complexity of atrial arrhythmia demands such a modeling approach.

When applied to arrhythmia, such models should be flexible enough to test various hypotheses on the expression of the etiology of the disease in the ECG. The simulated epochs should be long enough to permit an appropriate statistical analysis of the activation patterns. Furthermore, the model should exhibit a behavior compatible with that observed in invasive mapping studies of AF.

The geometry of the human atria used in this study was derived from magnetic resonance images (MRI). It includes the details of the entries and exits of the vessels as well as of the locations of the valves connecting the atria to the ventricles, which form natural barriers to the activation process. The electric propagation of the cardiac impulse was derived by solving a set of reaction-diffusion equations based on a detailed ionic model of the cell membrane kinetics. This set of equations links the local transmembrane potential to the sum of the ionic currents resulting from the activity at the membranes. Ideally, this set of equations would have to be solved for all of the myocytes involved (~2×10^8), which

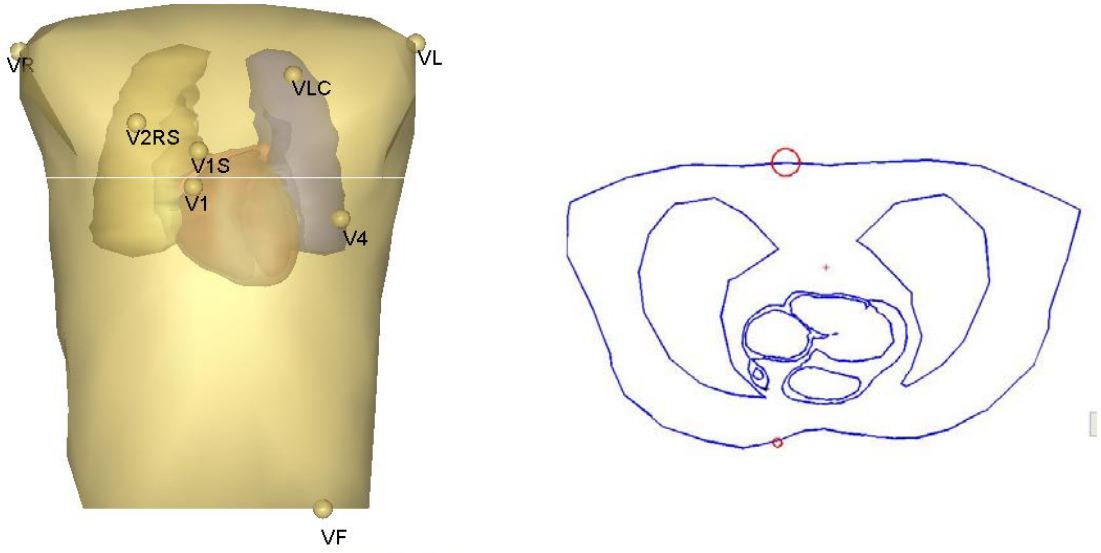

Figure 5. Left panel: Geometry of thorax, lungs, ventricles and atria as used in the example. The dots represent the locations of a nine-electrode-based lead system, which has been optimized for the analysis of the atrial VCG [23]. It in includes one electrode on the back, the position of which is shown on the right panel. The horizontal line indicates the level of the cross-section of the thorax shown on the right. **Right panel:** Cross-section through the thorax at the level of electrodes V1 and the one on the back. Note the relatively small distance between the apex of the right atrial appendix and the electrode sensing V1.

is clearly impractical. Instead, the system is solved numerically on the nodes of a grid defined in the interior of the atrial wall, specified at approximately 800,000 nodes. The solution produces the time courses of the transmembrane potentials, from which the current sources generating the observed potentials can be derived.

This activation model has been applied in the simulation of normal atrial activation, atrial flutter and atrial fibrillation. In all cases the models yielded signals that were in agreement with experimentally observed data. In addition, it has been applied to the development of various signal analytical tools. A full overview of these activities can be found on the website cited above. The most recent activities of the group include the research into vectorcardiography-based types of analysis. The remaining part of this paper explores the situations in which this type of approach might prove valuable.

Dipolar Source Descriptions during AF

Model-based as well as electrophysiology-based studies have previously corroborated the use of either point-source volume current densities throughout the myocardial tissue or equivalent double layers (EDL) sources at the closed surface bounding the myocardium [25]. The analysis of simulated activation sequences during AF has revealed a diversity of such patterns, associated with different substrates [26]. Most of these patterns, due to their spatial complexity, do not invite the use of a dipolar source description, in particular not for describing electrograms close to the myocardium. However, in some of the sequences, a small number of dominant, rotor-like sequences have been observed. It is for these types of AF that the current dipole may be used, in particular for describing the potentials at some distance, as are the ECGs. As is well known, the potential field generated by an arbitrary source configuration tends to be dominated more and more by its dipolar component the further one moves away from the source. The analysis of such rotor–like activities becomes easier the longer they exhibit spatial stationarity.

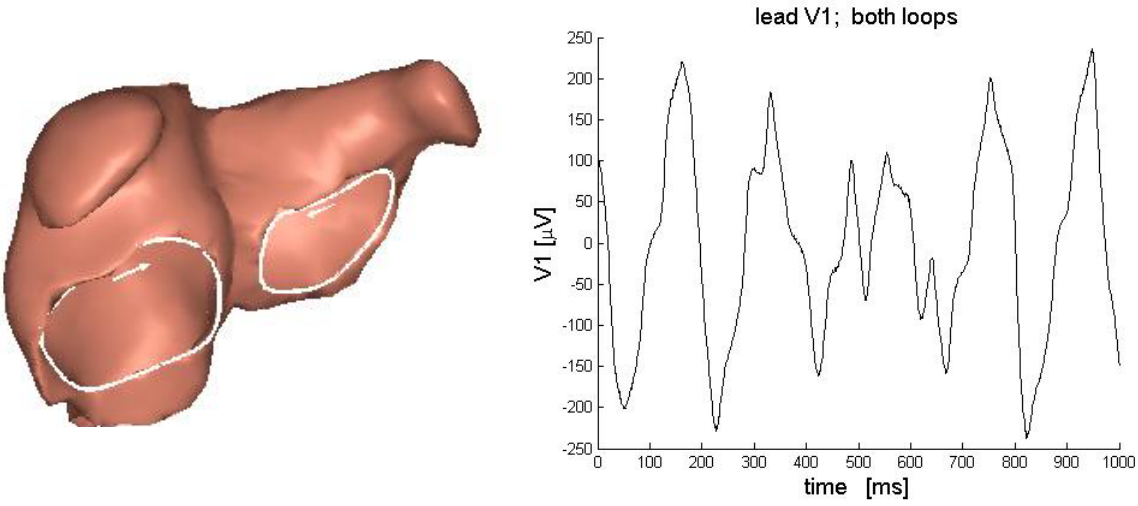

Figure 6. Left panel: Thick, white lines: contour along which two unit current dipoles travel, directed along the contours, pointing in the direction of propagation, while both moving at a velocity of 0.7 m/s. **Right panel:** Potential of lead V1 in a homogeneous conductor thorax model (left panel of Figure 6) as generated by these two dipoles. Compare the location of the apex of the right atrial appendix with that shown on the right panel of Figure 5, indicating that, in this subject, a substantial part of the atrial source activity took place at a level below that of electrode V1.

An Example

In the following example, two stable, rotor-like activities are assumed to be revolving around the mitral valve and the tricuspid valve area. The geometry involved has been derived from magnetic images of a 22-year-old human male [24] (Figures 4 and 5). The entire electric activity of the rotor is represented by two equivalent current dipole sources of unit strength, directed along the respective orifices, both revolving at a uniform velocity of 0.7 m/s, respectively (left panel of Figure 6). As they move along, their dipole components in 3D space vary with time. The lengths of the contours are 108.4 and 136.6 mm for the contours marked MV and TVC (left panel of Figure 4), respectively. The activity of the sources was periodic, with frequencies of revolution of 5.10 and 4.63 revolutions per second (RPS) of the rotors MV and TVC, respectively.

The potential field generated by these sources on the thorax surface of the homogeneous, bounded volume conductor (Figure 4) was computed by means of the BEM. The resulting potential at the sensing electrode of lead V1 is shown on the right panel of Figure 6.

The nature of this signal, over a period of 1 s resembles that of clinical recordings taken from AF patients, but here generated by just two, completely periodic phenomena. The interpretation of the significance of the temporal nature of the signal on the basis of just one such a record is clearly impossible. It is here that the spatio-temporal source nature might be explored, and the model of multiple, dominant rotors as implied in the (revolving) current dipole model is the most simple one.

To appreciate this, we first look at the strengths over time of the individual dipole components. Those of the example treated here are shown on the left panels of Figure 7. To the right of this are shown the individual contributions of the two revolving dipoles. Their sum is the potential documented on the right panel of Figure 6. Note the periodic nature of these signals, yet, when simultaneously active, the generated wave form V1 has an almost chaotic appearance, as is shown on the right panel of Figure 6.

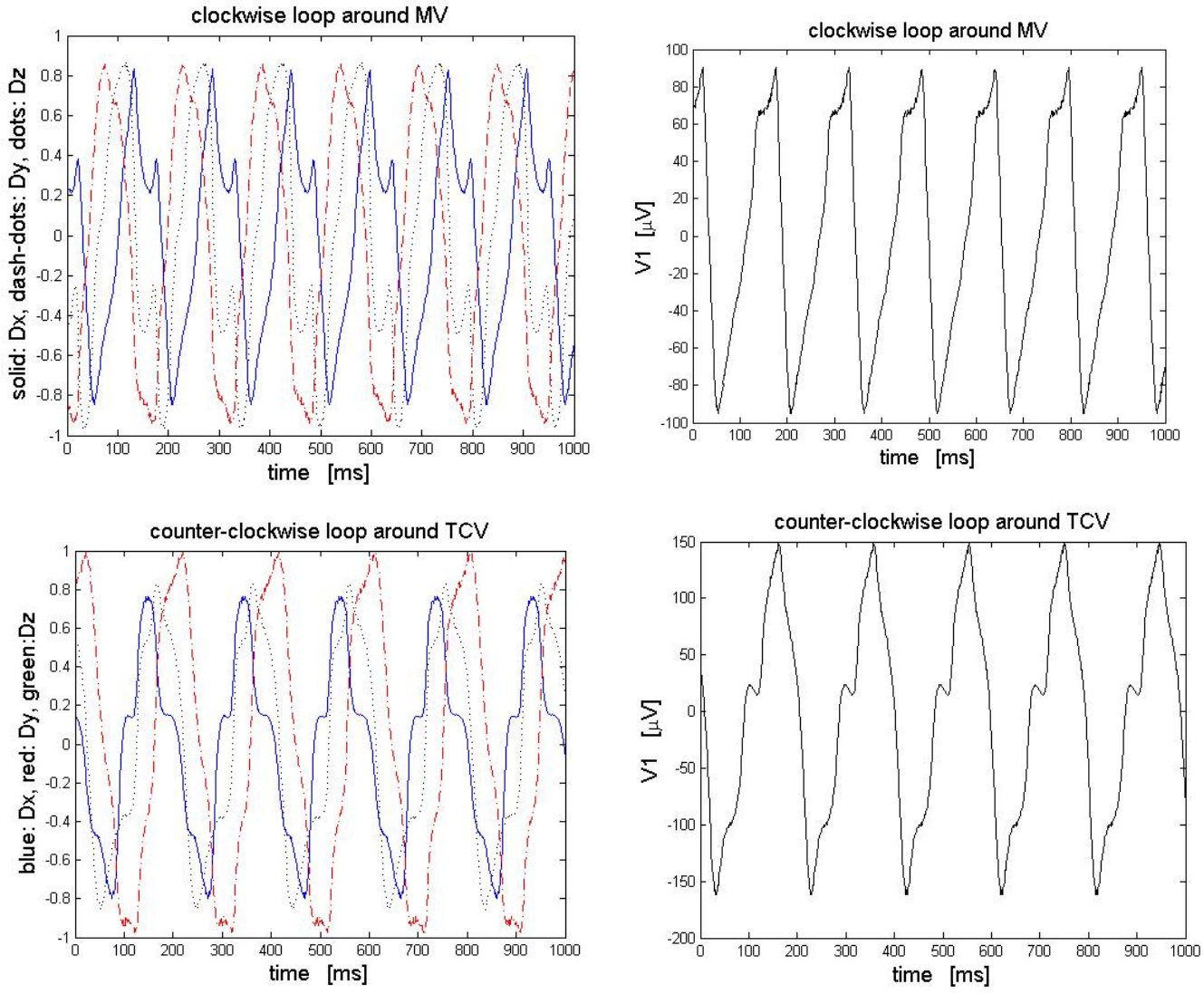

Figure 7. Panels referred to in matrix notation. **Panel 1,1:** The three components [$D_x(t)$. $D_y(t)$, $D_z(t)$] of a unit-strength dipole while revolving along contour MV. **Panel 1,2:** potential at V1 generated by the dipole along MV. **Panel 2,1:** The three components [$D_x(t)$. $D_y(t)$, $D_z(t)$] of a unit-strength dipole while revolving along contour TCV. **Panel 2,2:** potential at V1 generated by the dipole along contour TCV.

Next we test the estimation of these dipole components on the basis of the potentials "observed" at a limited set of electrodes, those of the OACG lead system, depicted on the left panel of Figure 5. This electrode montage was designed specifically, aimed at the analysis of atrial signals [23]. The matrix **M**

required for estimating the dipole, dedicated to the example treated here, was computed by means of the procedure outlined in the first part of this paper. For the single, fixed dipole involved, a position halfway between the centres of gravity of the two loops MV and TCV was chosen.

The results of the application of this matrix to the potentials generated by the separate activities along the contours as well as to the potentials resulting from their combined activity, the estimated dipole components of the VCG, are shown in Figure 8.

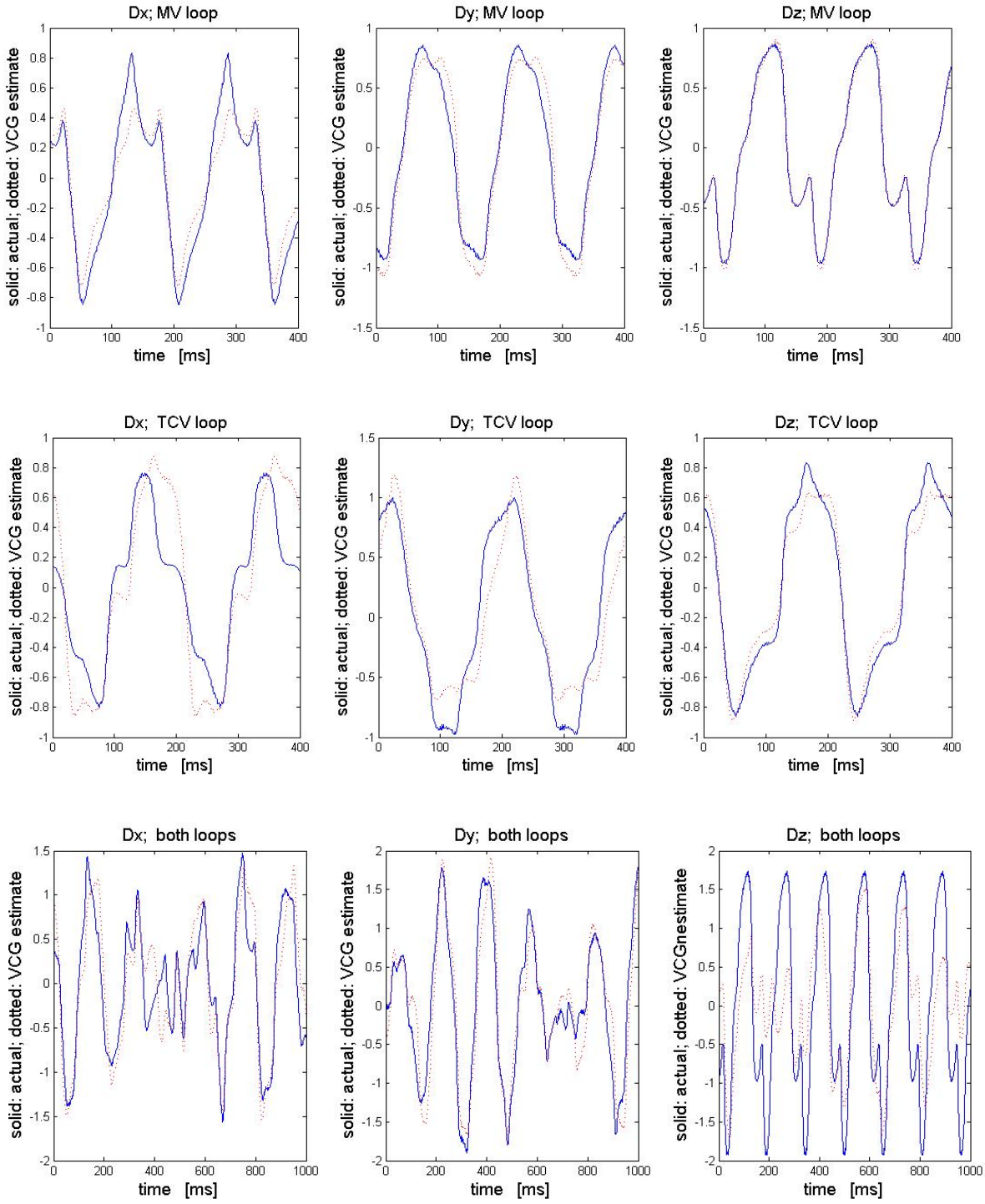

Figure 8. Upper row: dipole components of the current diplole revolving along the contour MV. Solid lines replicate the data on the upper left panel of Figure 7. Dotted lines are the dingle dipole estimates based on the

OACG lead signals. **Middle row:** as upper row, but here for contour TCV. **Lower row:** as in the rows above, but now based on the OACG signals during the simultaneous activity of both rotors.

DISCUSSION

The results presented in Figure 8 indicate that rotor-like propagation over the atrial surface can be identified by means of the analysis of the $X(t)$,$Y(t)$, $Z(t)$ signals of the VCG, the estimates of the components $D(t)$,$D(t)$, $D(t)$ of the dipolar source vector. The latter are the estimates of the total source distribution throughout the myocardium in the form of a single equivalent dipole.

If just a single rotor is active, as in the case of atrial flutter, the accuracy of the estimated dipole trajectory is high, as can be seen in the traces shown on the upper two panels of Figure 8. On the basis of the dipolar components, the trajectory along which the activity rotates can be established in a straightforward manner.

If multiple, dominant rotors are involved, as is the case during some types of AF, the situation is more complex. This is obvious from the results shown on the lower panels of Figure 8, in which no immediate interpretation of the components of the single, estimated dipolar activity is possible. This comes as no surprise since, after all, two such revolving source dipoles were involved. The solution here, which has been explored in a recent study [27], is based on the fact that the number of revolutions per second of individual rotors tends to be distinct. Filtering in the frequency domain in order to identify and separate individual rotor-like activity then becomes feasible. Longer periods of quasi-stationarity of the individual rotors will enhance the quality of the source identification performed by such filtering procedures. In the study reported, [27] , up to three such, simultaneously active rotors could be identified in this manner.

The quality of these estimation (inverse) procedures increases with the number of electrodes sampling the spatial aspects of the electric source activity. If just a few electrodes are feasible, their distribution over the thorax needs to be tuned to the application in hand. The OACG lead system, shown in Figure 5, has nine electrodes, five of which (V1, V5, VR,VL and VF) are the same as used in the standard 12-lead system.

The quality of the estimate also depends on the matrix **M** involved in converting the observed signals to the dipole estimates. The procedure for computing **M,** as is discussed in the first part of this paper, is fast and adequate, and can be easily applied to any preferential location of the single, fixed dipole location involved in designing **M**.

The performance of the developed models of the electric sources during AF and of the electric volume conduction effects suggests they have reached the required level of quality to allow us to start applying these toward the improvement of current diagnostic tools for AF.

REFERENCES

[1] W. B. Kannel, R. D. Abbott, D. D. Savage, and P. M. McNamara, "Epidemiologic features of chronic atrial fibrillation: the Framingham study," *N Engl J Med*, vol. 306, pp. 1018-22, 1982.

[2] Y. Miyasaka, M. E. Barnes, B. J. Gersh, S. S. Cha, K. R. Baily, W. P. Abhayaratna, J. B. Seward, and T. S. M. Tsang, "Secular Trends in Incidents of Atrial Fibrillation in Olmsted County, Minnesota, 1980 to 2000, and Implications on the Projections for Future Prevalence," *Circulation*, vol. 114, pp. 119-125, 2006.

[3] V. Fuster, L. E. Ryden, R. W. Asinger, D. S. Cannom, R. L. Crijns, R. L. Frye, J. L. Halparin, G. N. Kay, W. W. Klein, S. Levy, R. L. McNamara, E. N. Prystowsky, L. S. Wann, and D. G. Wyse, "ACC/AHA/ESC guidelines for the management of patients with atrial fibrillation," *Eur Heart J*, vol. 22, pp. 1852-1923, 2001.

[4] M. Haissaguerre, P. Jais, D. C. Shah, A. Takahashi, M. Hocini, G. Quiniou, S. Garrigue, A. L. Mouroux, P. L. Metayer, and J. Clementy, "Spontaneous initiation of atrial fibrillation by ectopic beats originating in the pulmonary veins," *N. Eng. J. Med.*, vol. 339, pp. 659-666, 1998.
[5] R. M. Gulrajani, F. A. Roberge, and P. Savard, "The Inverse Problem of Electrocardiography," *Comprehensive Electrocardiology*, vol. I, pp. 237-288, 1989.
[6] R. M. Gulrajani, F. A. Roberge, and G. E. Mailloux, "The Forward Problem of Electrocardiography," in *Comprehensive Electrocardiology*, vol. I, P. W. Macfarlane and T. T. V. Lawrie, Eds. Oxford: Pergamon Press, 1989, pp. 197-236.
[7] R. M. Gulrajani, *Bioelectricity and Biomagnetism*. New York: John Wiley & Sons, 1998.
[8] R. Plonsey and R. C. Barr, *Bioelectricity: A Quantitative Approach*. New York: Springer, 2007.
[9] W. Einthoven, G. Fahr, and A. de Waart, "Űber die Richtung und die manifeste Grősse der Potential Schwankungen im menschlichen Herzen und űber den Einfluss der Herzlage auf die Form des Elektrokardiogramms," *Pflugers Arch (Translated: Am. Heart J. 1950; 40: 163-211.)* vol. 150, pp. 275-315, 1913.
[10] A. Waller, " A demonstration on man of the electromotive changes accompanying the heart's beat," *J Physiol*, vol. 8, pp. 229-234, 1887.
[11] H. C. Burger, "The Zero of Potential: A Persistent Error," *Am Heart J*, vol. 49, pp. 581-586, 1955.
[12] D. B. Geselowitz, "The Zero of Potential," *IEEE Engineering in Medicine and Biology Magazine*, vol. 17, pp. 128-132, 1998.
[13] R. Plonsey, *Bioelectric phenomena*. New York: McGraw-Hill, 1969.
[14] B. M. Horáček, "Lead Theory," in *Comprehensive Electrocardiology*, vol. I, P. W. M. a. T. T. V. Lawrie, Ed. Oxford: Pergamon Press, 1989, pp. 291-315.
[15] T. F. Oostendorp and A. van Oosterom, "Source parameter estimation in inhomogeneous volume conductors of arbitrary shape," *IEEE Trans. Biomed. Eng.*, vol. BME-36, pp. 382-391, 1989.
[16] G. E. Dower, "An Arrhythmia Clarified by Polarcardiography " *J Electrocardiol*, vol. 3, pp. 231-238, 1970.
[17] A. van Oosterom, R. Hoekema, and G. J. Uijen, "Geometrical factors affecting the interindividual variability of the ECG and the VCG," *J Electrocardiol*, vol. 33 S, pp. 219-227, 2000.
[18] D. Gabor and C. V. Nelson, "The determination of the resultant dipole of the heart from measurements on the body surface," *J. Appl. Phys.*, vol. 25, pp. 413-416, 1954.
[19] E. Frank and C. F. Kay, "Frontal plane studies of Homogeneous Torso Models," *Circulation*, vol. 9, pp. 724-740, 1954.
[20] P. W. Macfarlane, "Lead Systems," in *Comprehensive electrocardiology: Theory and Practice in Health and Disease*, vol. 1, P. W. Marfarlane and T. D. Veitch, Eds. Oxford: Pergamon Press, 1989, pp. 315.
[21] H. C. Burger and J. B. v. Milaan, "Heart Vector and Leads," *Br. Heart J.*, vol. 8, pp. 157-161, 1946.
[22] E. Frank, "An accurate, clinically practical system for spatial vectorcardiography," *Circulation*, vol. 13, pp. 737-49, 1956.
[23] A. van Oosterom, Z. Ihara, V. Jacquemet, and R. Hoekema, "Vectorcardiographic lead systems for the characterization of atrial fibrillation
" *J Electrocardiol*, vol. 40, pp. 343.e1-343.e11, 2007.
[24] P. M. van Dam and A. van Oosterom, "Volume conductor effects involved in the genesis of the P wave," *Europace*, vol. 7, pp. S30-S38, 2005.
[25] A. van Oosterom and V. Jacquemet, "Genesis of the P wave: Atrial signals as generated by the equivalent double layer source model," *Europace*, vol. 7, pp. S21-29, 2005.
[26] M. Lemay, J. Vesin, V. Jacquemet, A. Forclaz, L. Kappenberger, and A. van Oosterom, "Spatial dynamics of atrial activity assessed by the vectorcardiogram: from sinus rhythm to atrial fibrillation," *Europace*, vol. 9, pp. vi109-vi118, 2007.

[27] C. Duchene, M. Lemay, J.-M. Vesin, and A. Van Oosterom, "Estimation of Atrial Multiple Reentrant Circuits from Surface ECG Signals Based on a Vectorcardiographic Approach " presented at Functional Modelling of the Heart, Berlin, 2009.